Effect of process parameters on the mechanical properties of wires produced from A356 aluminum alloy chips by Continuous Friction Stir Extrusion: Experiments and numerical simulation

Simone Amantia, Davide Campanella, Riccardo Puleo, Gianluca Buffa *, Livan Fratini

Department of Engineering, University of Palermo, Viale delle Scienze, 90128, Palermo, Italy

ARTICLE INFO

Keywords:
Friction Stir Extrusion
Solid bonding criteria
Aluminum alloys
Chips recycling
F.E.M

ABSTRACT

Recycling of metals is becoming crucial from an economic and environmental point of view. The solid-state recycling process Continuous Friction Stir Extrusion was used to produce wires out of A356-T6 chips. The mechanical properties of the produced wires were explored by varying the main process parameters. Characterization involved Vickers hardness tests, tensile tests, grain size measurements, and fracture surface analysis. It has been found that it is possible to achieve 77 % of the Ultimate Tensile Strength (UTS) and 92 % of Vickers hardness with respect to the as-fabricated A356 alloy. The average grain size increases with the tool rotational with values ranging from about 9 μm to about 11 μm. A 3D dedicated numerical model was used to predict the distributions and histories of primary field variables, and to calculate the Piwnik-Plata parameter, fostering a more in-depth understanding of the process mechanics. This allows for the precise prediction of unacceptable product quality of the bonding when the Plata and Piwnik parameters are low. Predicted temperature close to the rotating tool should reach 400 °C while the cochlea temperature should be below 100 °C for sound wires production thus avoiding early chip bonding and process failure.

1. Introduction

The extraction of primary resources holds growing importance from both economic and environmental standpoints. Focusing on the environmental aspect, CO_2 emissions, and energy consumption during the production phase reach a significant amount per year, comprising over a quarter of the global CO_2 output [1]. Projections by Gutowski et al. [2] suggest a substantial surge in aluminum demand in the future, potentially tripling current levels. Improving the efficiency of primary production methods and recycling processes is imperative based on these findings. Tolio et al. [3] propose that the aforementioned challenges necessitate exploring options such as product repairing, remanufacturing, and recycling. Anyway, as emphasized by Atherton [4], recycling stands out as the leading strategy for metals, due to its substantial economic and environmental advantages, given that numerous metals can undergo multiple reprocessing cycles. Ingarao [5] demonstrates that aluminum alloys are well suited to recycling through remelting with 90 % of primary energy saving. However, it is noted that conventional industrial remelting procedures exhibit low efficiency. In the 1940s, solid bonding phenomena were proposed and patented in the United States to recycle metals. For the development of new processes focusing on the recycling of waste materials, the phenomenon of high plastic deformation is currently being extensively studied. The solid bonding phenomenon requires (i) high-pressure conditions to bring all the involved elements into intimate contact, (ii) high temperature, which can be due to the heat dissipated by the friction between the main elements of the process (e.g. friction-based processes), and (iii) a certain time to allow for the correct processing of all the material. These conditions must be met for solid bonding activation to occur. In order to use this technique for the recycling of aluminum scraps, it is necessary to consider the difficulties caused by the high hardness and chemical instability of the surface oxide layer. Processes based on severe plastic deformation can effectively destroy the surface oxide layer of the scraps by subjecting the material to significant strain, thereby allowing for the formation of metal bonds [6]. Mathematical models were used by Cooper and Allwood [7] to summarize the impact of deforming conditions on forming solid bonds.

There are two types of Solid-State Recycling (SSR) technologies: (i) Spark Plasma Sintering (SPS), a powder metallurgy approach, for which Paraskevas et al. [8] illustrated the efficacy in directly joining aluminum

Table 1
Mechanical, physical properties, and chemical composition of A356.

Heat Treatment	YS [MPa]	UTS [MPa]	HV	Elongation	`
F	83	159	67	6 %	
T6	207	278	108	6 %	

Chemical composition % w/w

Al	Cu	Fe	Mg	Mn	Si	Ti	Zn	Each
91.1 - 93.3	≤ 0.20	≤ 0.20	≤ 0.25 – 0.45	≤ 0.10	6.5 - 7.5	≤ 0.20	≤ 0.10	≤ 0.20

Fig. 1. Shape and dimensions of metal chips used during the experimental campaign.

and magnesium alloy chips to produce cast semi-finished products; (ii) Extrusion-based processes, whose shape flexibility and productivity are higher. The following factors have been identified as important in the extrusion process to obtain a solid joint and improved mechanical properties [9]: (i) the severe plastic deformation the material undergoes breaks the oxide film on the surface of the chips, allowing a metal-to-metal bond; (ii) the concurrent effect of temperature and strain causes changes to the microstructure of the material and therefore also to the mechanical properties of the final recycled product.

Different approaches can be employed to reach these process conditions, such as direct hot extrusion, Friction Stir Extrusion (FSE), Equal Channel Angular Pressing (ECAP), or their combination. According to Liu et al. [10], around 8 % of semi-finished products are aluminum wires and profiles. Additionally, waste generated during the cutting process constitutes a significant portion of overall industrial aluminum waste, amounting to 18 %. In these operations, Friction Stir Extrusion (FSE), also known as Friction Stir Backward Extrusion (FSBE), can play a crucial role. The method originates from friction welding and enables the conversion of metal chips into a solid wire. In this procedure, a rotating die is moved near a hollow chamber containing the chips for processing. Chips are softened by heat generated due to the frictional forces between them and the rotating die. Furthermore, the movement of the die causes a strong deformation based on the extrusion ratio, which can be defined as the ratio of the rotating die's diameter to the die cavity's diameter. Under these circumstances, the material reaches the conditions for solid bonding, leading to the activation of backward extrusion along the tool axis.

Some of the authors have investigated the FSE process and developed a numerical FEM model to improve the process by predicting the bonding conditions effectively [11,12] and the energy requirements for producing aluminum alloy wires are examined [13]. The electrical energy consumption is measured for different process parameters. FSE demonstrates a significant energy reduction, up to 74 % compared to conventional methods and 63 % compared to ECAP routes. The FSBE technique was examined in 2019 by Jamali et al. [14], with a particular emphasis on how the process affected the mechanical characteristics and microstructure of the aluminum alloy AA6063. The same authors [15] also highlighted that rotational speed has an impact on the machined

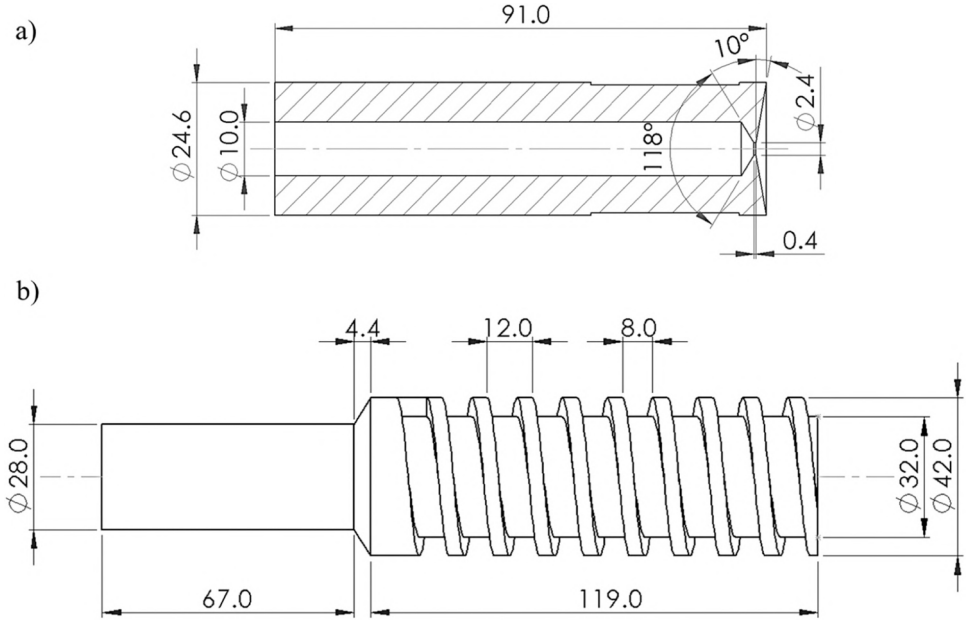

Fig. 2. (a) Geometry dimensions of rotating tool and (b) geometry dimensions of redesigned cochlea.

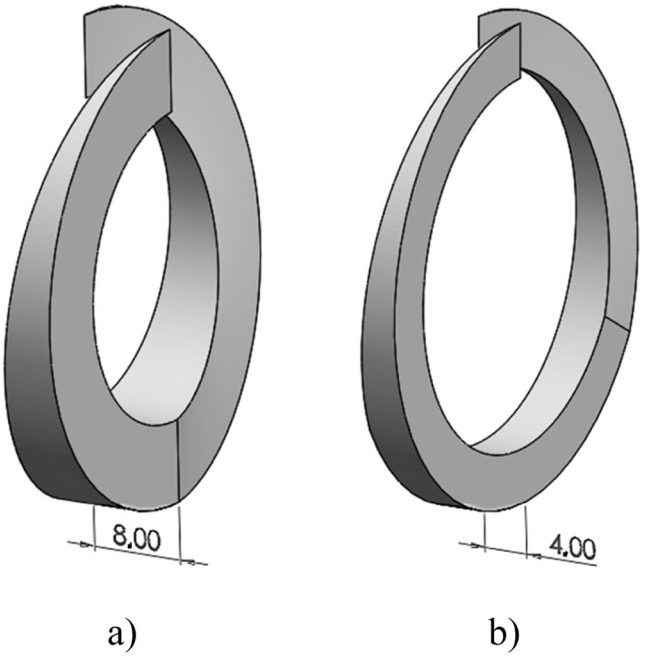

Fig. 3. Different volumes available for chips in the old (a) and (b) redesigned geometry cochlea.

Table 2
Volume of chips introduced for every rotation of cochlea.

	V_i (mm^3)	Mass, m_r (g)	V_r (mm^3)
Old design	3355	3.9	1452
New design	1356	1.6	596

Table 3
Case studies investigated.

ID	ω tool [rpm]	ω cochlea [rpm]
a	915	21
b		42
c		84
d	1250	21
e		42
f		84
g	1600	21
h		42
i		84

material's microstructure, where higher speeds lead to an accidental disposition. Tahmasbi et al. [16] applied Friction Stir Extrusion (FSE) to chips of AA7022, observing a decrease in corrosion resistance as the tool rotation speed increased. Some of the authors investigated the effects of varying rotational speeds and vertical loads on the production of wires from AA7022 waste [17]. Their study observed a degradation in surface quality with increasing rotational speed, along with a decrease in vertical load. Behnagh et al. [18] carried out a combined numerical and experimental study on FSE, utilizing a three-dimensional finite element model to predict the distribution of important thermo-mechanical field variables. Akbari et Asadi [19,20], investigated the possibility of producing brass wire through FSE and developed a computational framework to forecast the three-dimensional material movement. Some authors [21] studied the extrusion of LM28 aluminum with silicon powder into tubes and evaluated their mechanical and wear properties through compression and wear tests. Gumaste et al. [22] demonstrated the feasibility of the Solid Stir Extrusion process using Al 6061-T6 as the feedstock material. The force and torque were correlated with microstructural and mechanical characterization. The idea of employing FSE to produce rare earths with high mechanical characteristics was investigated by Li et al. [23]. Furthermore, Li et al. [24] introduced a

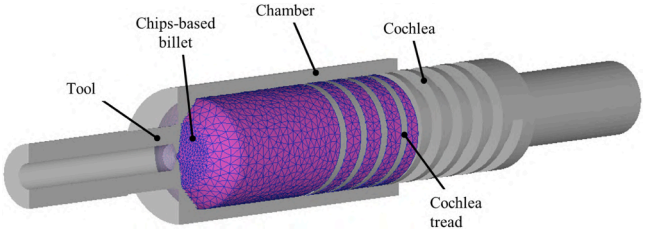

Fig. 5. 3D FEM model of the CFSE process: section of the tool, chips-based billet, chamber, and treads of the cochlea.

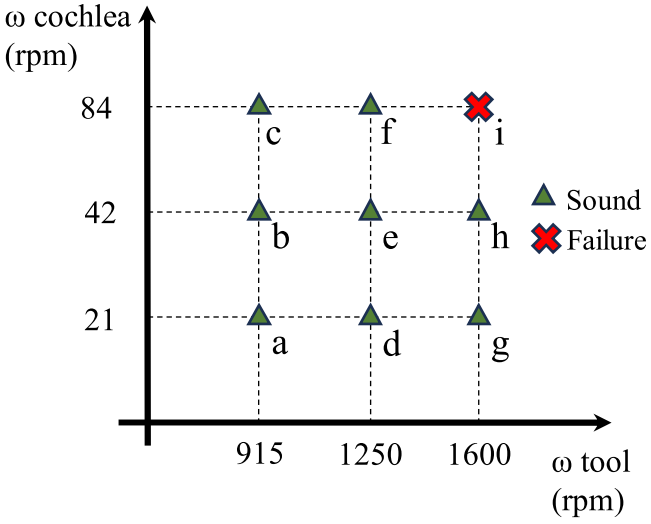

Fig. 6. Process window highlighting sound and failed tests.

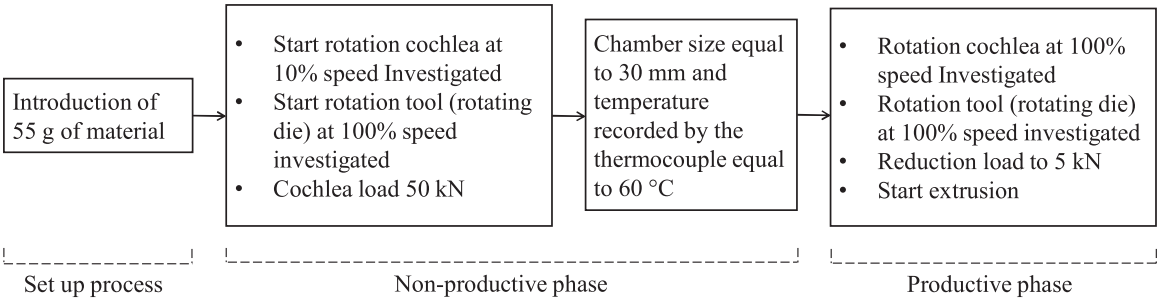

Fig. 4. Experimental procedure.

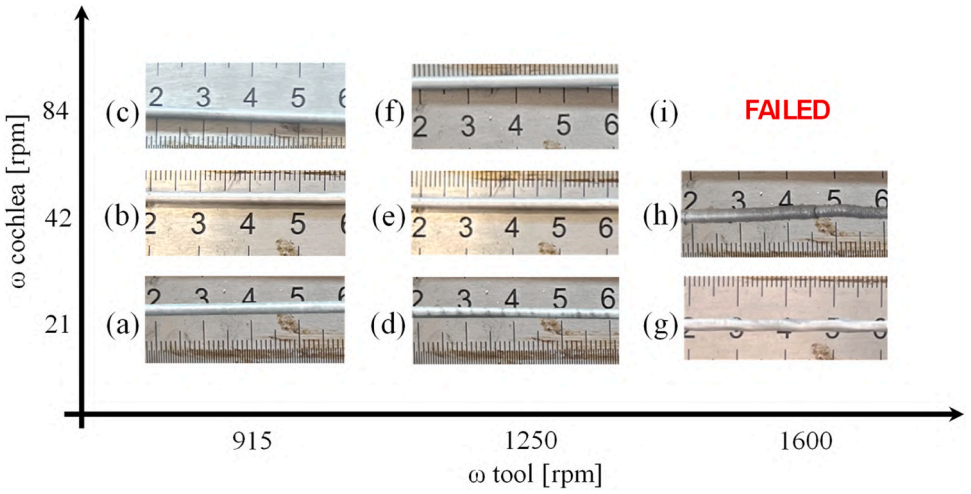

Fig. 7. Longitudinal view (a) ID-a, (b) ID-b, (c) ID-c, (d) ID-d, (e) ID-e, (f) ID-f, (g) ID-g, (h) ID-h, and (i) the failure of ID-i.

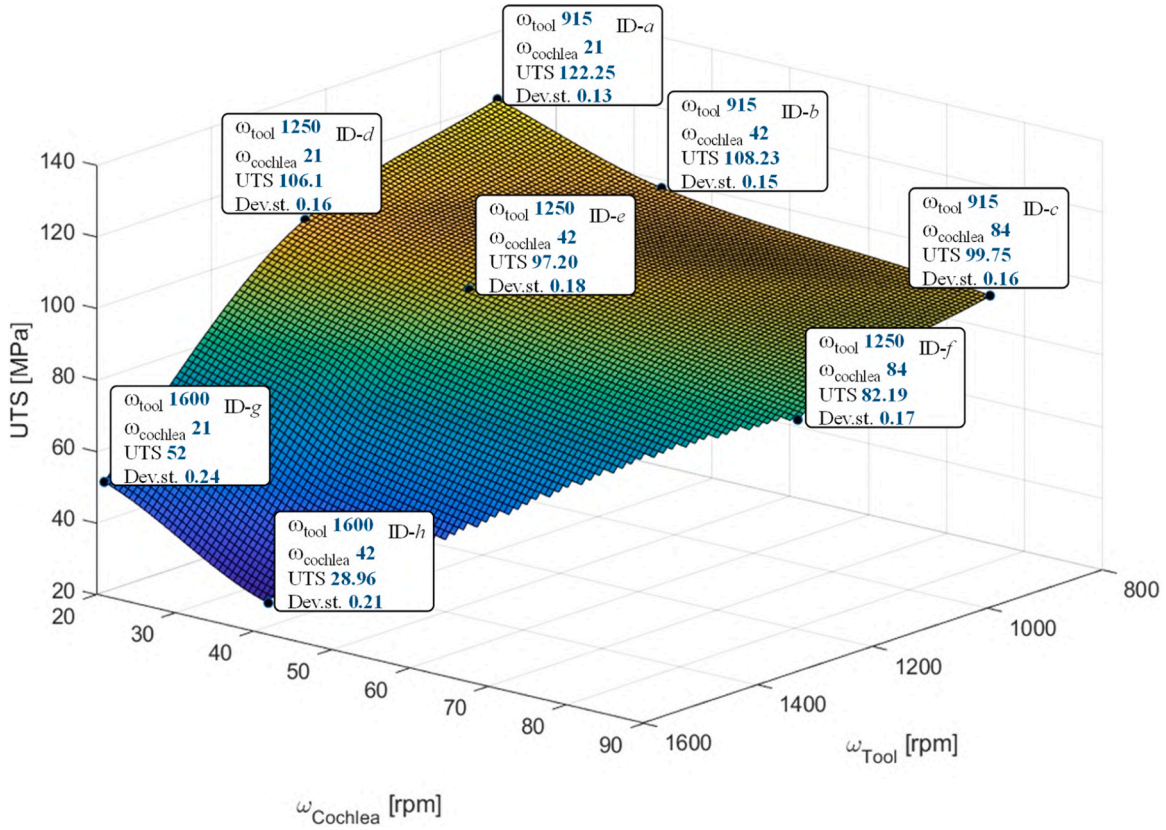

Fig. 8. Ultimate Tensile Strength (UTS) of the produced wires correlates with both the rotational speed of the cochlea and the rotational speed of the rotating die.

meshless numerical model of the FSE process for aluminum wire production based on Smoothed Particle Hydrodynamics (SPH). Jarrah et al. [25] have developed and validated a Coupled Eulerian-Lagrangian thermomechanical model to simulate the FSBE process of Mg AZ31B tubes. Recently, it has been shown that the gradient distribution of reinforcement particles controlling the mechanical properties of the resultant composite material can be achieved in the production of Al/SiC wire by FSBE [26], as studied by Jamali et al.

From the SoA presented it is observed all the techniques used have a discontinuous production phase. In this way, the limited amount of chips that can be charged for each process run results in a limited wire/rod maximum length. This statement holds true also for the FSE/FSBE process. Moreover, additional maintenance tasks, such as clearing leftover material in dead zones, are frequently required in between extrusions to return the hopper to its original condition. Continuous Solid Extrusion (CSE) can greatly increase wire productivity and energy efficiency. Widerøe and Welo [27] first proposed the concept of the CFSE process. The created machine's primary features, which are drawn from those used for polymer extrusion, can be summed up as follows: The raw material is conveyed via a motor reducer, which propels a horizontal screw situated within a heated container; the material is heated concurrently by frictional forces, deformation forces, and contact with the machine's preheated walls. At the end of the screw, another heated extrusion chamber completes the recycling process, producing a solid

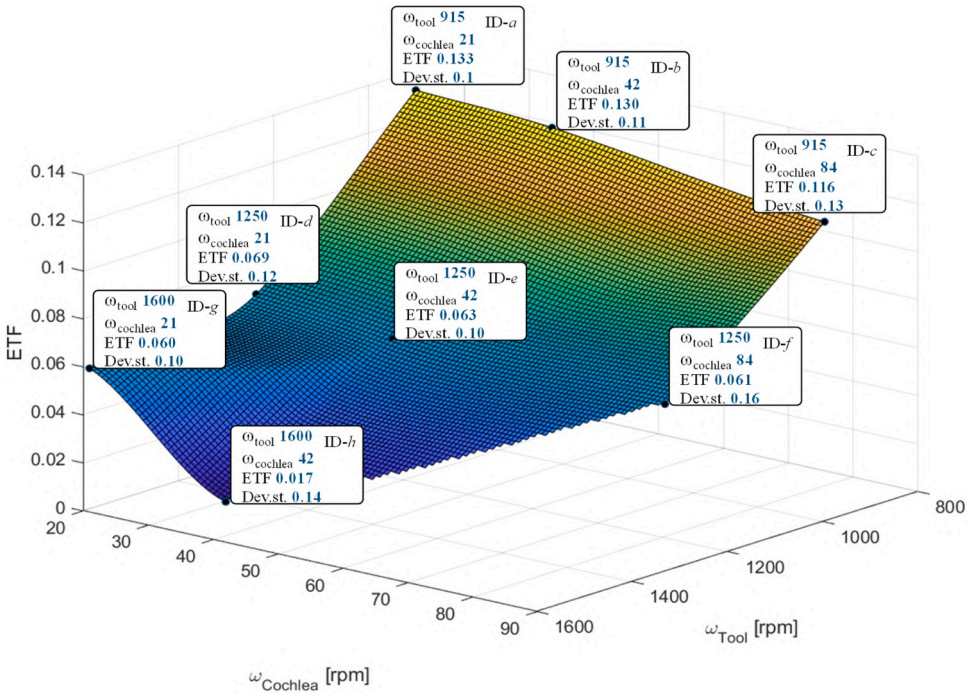

Fig. 9. The elongation to fracture of the produced wires varies with both the rotational speed of the cochlea and the rotational speed of the tool.

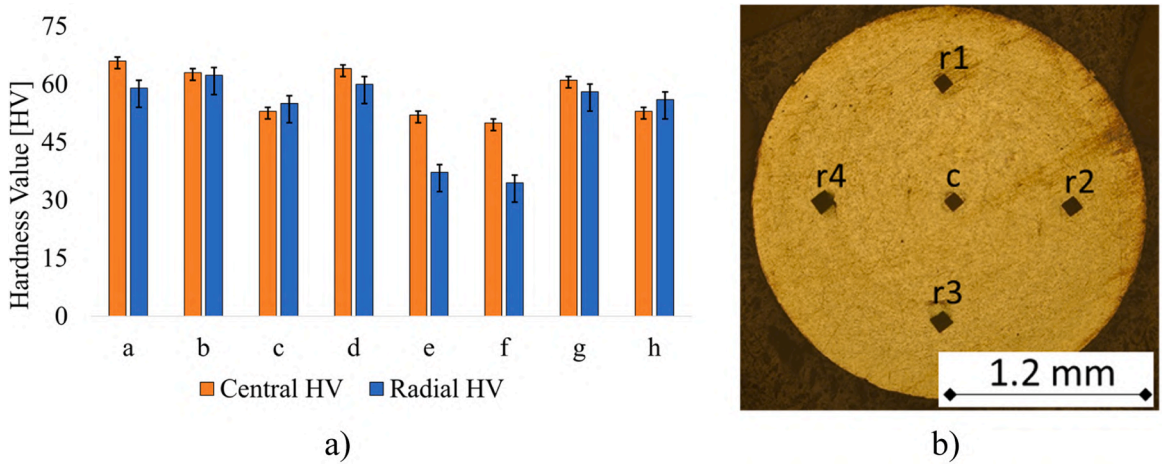

Fig. 10. (a) Micro Hardness results for the tested wires, (b) OM image of the indentations.

wire. Skorpen et al. [28] proposed an empirical model to quantify the stresses to which the scraps are subjected through the process. Significantly, the procedure entails an external heating step along with heating generated by frictional forces, thus partially reducing the energetic advantage of the process over other solid-state techniques. Finally, it is important to note that the material is provided in granular form in both [27] and [28], necessitating associated treatment when starting from machining chips. Some of the authors presented the Continuous Friction Stir Extrusion (CFSE) process [29], designed to overcome the shortcomings of FSE. In this way, it is possible to increase the process productivity by obtaining long wires, which are more suitable for many applications such as the Wire Arc Additive Manufacturing (WAAM) technology [30]. Indeed, a horizontal screw transports the raw material in the form of chips, similar to the screw extrusion process. The material is compressed by the rotating screw until it is extruded from the rotating head under the appropriate bonding conditions.

Being the CFSE process still relatively new, only a very limited number of papers is found in the literature, and research is needed to understand the underlying mechanisms governing their mechanical performance, thereby facilitating their widespread adoption in diverse industrial applications requiring high-strength and ductile wire materials.

In this paper, an experimental campaign was carried out with the aim to highlight the effect of the main process parameters, i.e. tool rotation and cochlea rotation, on the mechanical and microstructural properties of the produced wires. A prototypal machine, previously developed by some of the authors [29], was partially redesigned and used for the experiments. A dedicated numerical model was established and used to highlight the distributions and histories of the main field variables. The Piwnik-Plata criterion was used to evaluate the soundness of the solid bonding obtained thus explaining the results obtained during the tensile tests.

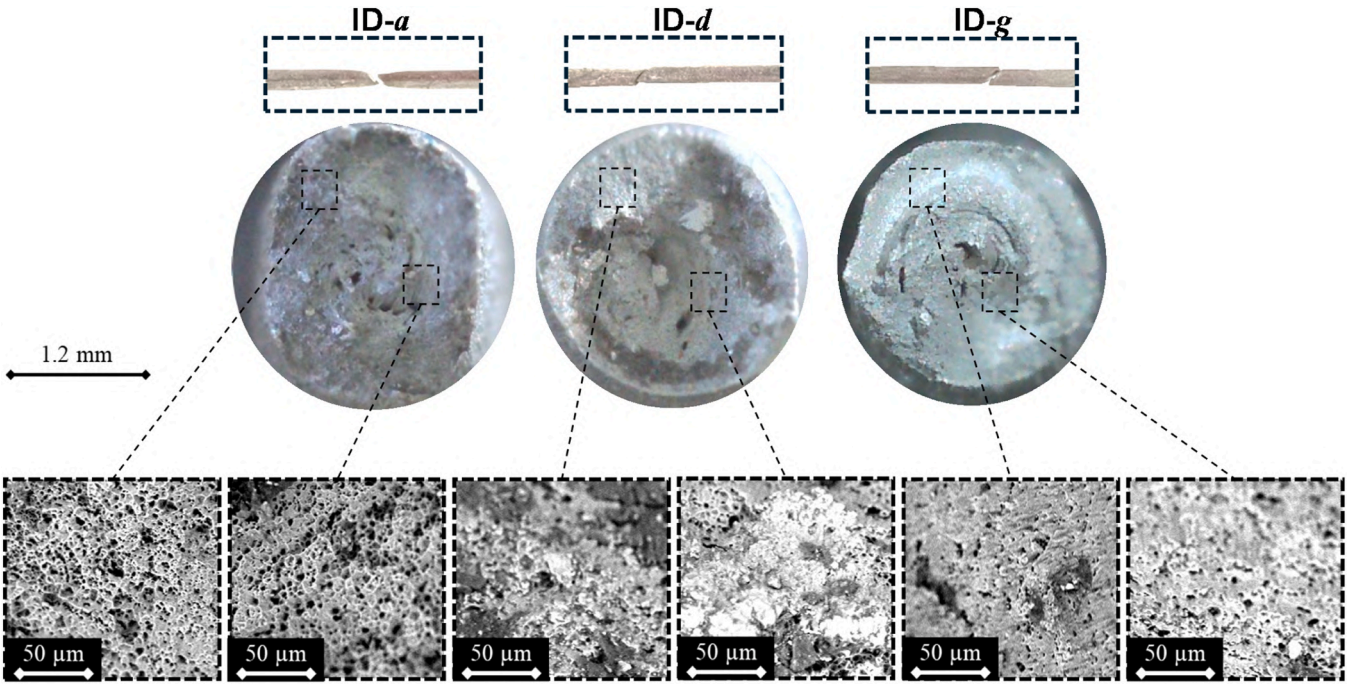

Fig. 11. Failure mode image and associated SEM image for ID-a, ID-d, and ID-g.

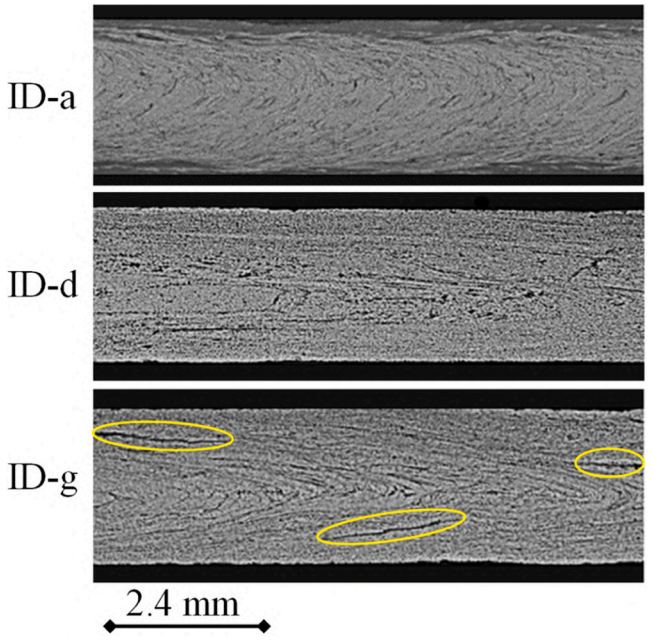

Fig. 12. Longitudinal section of the obtained wires for case studies ID-a, ID-d, and ID-g.

2. Materials and methods

2.1. Experimental activity

Aluminum alloy A356-T6 was used as the starting material for Continuous Friction Stir Extrusion (CFSE). Table 1 shows the mechanical properties and chemical composition of the material used [31,32]. Aluminum-silicon composites are widely used in the automotive industry not only because they can be effectively cast into complex structures, but also because of their wear resistance, lightweight, and good strength. For these reasons, A356-T6 is broadly used in the production of different automotive parts, such as engine blocks and wheels [33]. For its distinctive properties, extensive research has been conducted over the past few years to explore its use in various manufacturing processes, including Selective Laser Melting (SLM) 3D printing [34]. In this way, the amount of chips produced by the industry for this material is considerable.

The sizes and shapes of the chips that were used to perform the process are highly variable as they are produced by both turning and milling in different processing conditions (Fig. 1). However, as observed by Tekkaya et al. [9], extrusion is not affected by the different shapes of chips of introduced material if the correct pressure, strain, and temperature values are reached.

The CFSE process was carried out on the prototype machine presented by Buffa et al. [35].

Fig. 2a shows the geometry of the rotating used tool made of H13 steel. The rotating tool has an extrusion hole size of 2.4 mm and an extrusion channel length of 0.4 mm. Fig. 2b illustrates a redesigned cochlea (with respect to the one presented in [31]) made of H13 steel.

The redesigned cochlea has a core diameter of 32 mm to ensure robustness and prevent failure caused by deformations during the process. The outer diameter is 42 mm, resulting in an extrusion ratio of 17.5. The redesign of the cochlea was needed to decrease the volume of material introduced during each cochlea rotation: this was achieved through a larger core diameter (i.e. 32 mm) compared to the previous one (i.e. 26 mm). Previous experimental studies have shown that when the extrusion chamber is set at a fixed dimension of 30 mm and the same rotation parameters are used as in the present study, the volume of material introduced exceeds the volume of extruded material. This indicates a need to reassess the extension of the extrusion chamber, as material accumulation occurs without extrusion. To overcome this problem, the thread pitch characterizing the cochlea was changed from 16 mm to 12 mm without changing the distance between two adjacent threads, which is 8 mm.

Fig. 3 shows how the volume of chips introduced decreases with each rotation of the cochlea.

The relative density (ρ_r) of the chips deposited by simple gravity fall is 0.44. To determine this value, a cylinder with a diameter of 75 mm and a height of 95 mm was used, with a volume of 419,697 mm^3. The

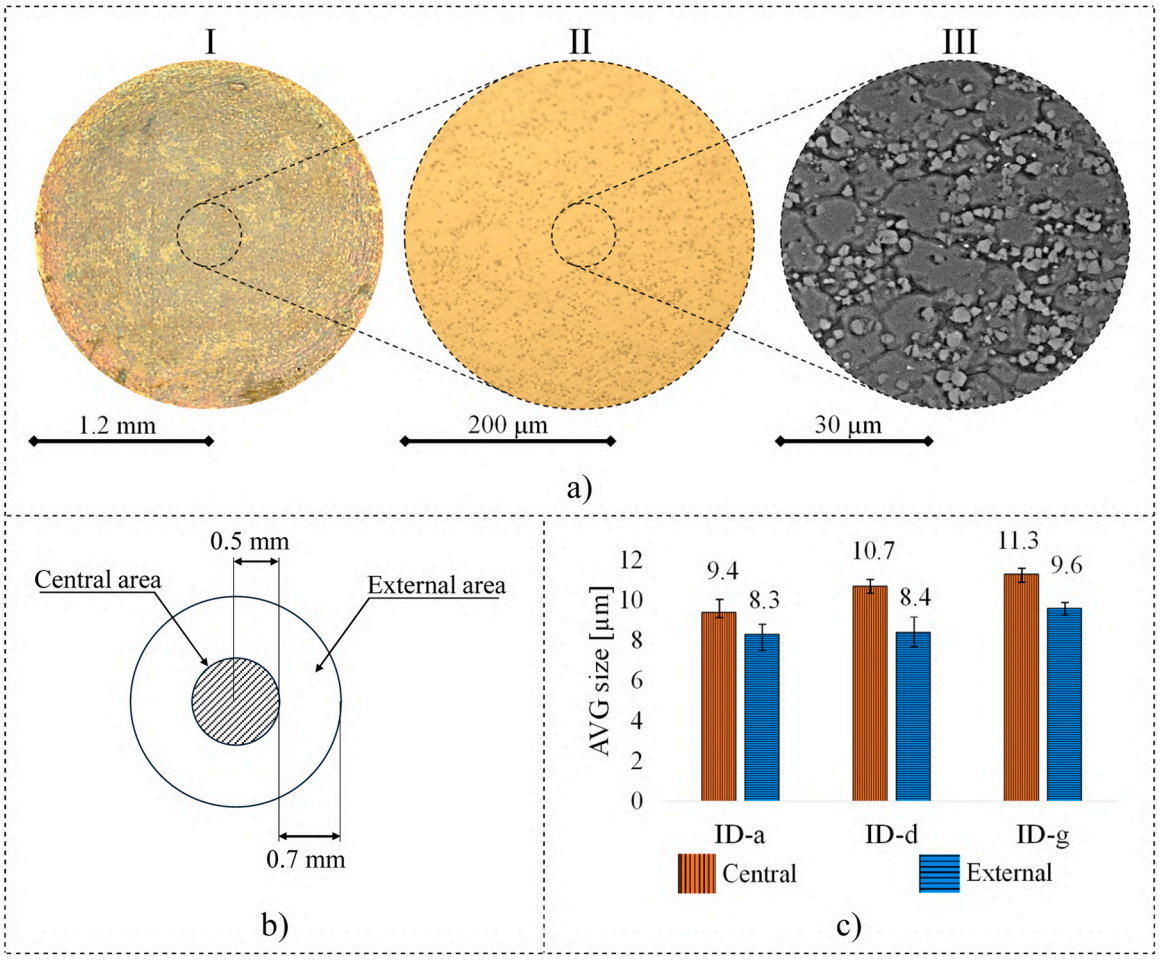

Fig. 13. (a) Microstructural analysis with (a.I) Optical microscope 5x (a.II) Optical microscope 20x and (a.III) SEM 2000x, (b) scheme of the analyzed zones, and (c) average grain size was measured for case studies ID-a, ID-d, and ID-g.

Table 4
ANOVA analysis results for UTS value.

Source	DF	Adj SS	Adj MS	F-Value	P-Value
ω tool	2	35323,2	17661,6	626792,52	0,000000
ω cochlea	2	4849,3	2424,6	86048,02	0,000000
ω tool* ω cochlea	4	875,2	218,8	7764,61	0,000000
Error	18	0,5	0,0		
Total	26	41048,2			

chips were deposited by gravity until the cylinder was filled. The material introduced into the volume was then weighed. The experiment was repeated five times and the average weight recorded was 495 g. It is possible to calculate the mass of chips introduced for each rotation (m_r), considering the density of the A356-T6 ($\rho_{A356\text{-}T6}$), the previously measured relative density (ρ_r), and the ideal volume (V_i) calculated through CAD techniques.

The actual volume of material introduced for each rotation for the two geometries, given the discrete nature of the chips (V_r) can be calculated with Eq. 1:

$$V_r = V_i \cdot \rho_r \quad (1)$$

Table 2 shows the ideal volume available for chips (V_i), the mass of chips introduced for each rotation (m_r), and the volume occupied by the chips introduced (V_r).

Based on the results of a preliminary campaign, aimed at demonstrating the feasibility of the process and highlighting the role of the main process parameters [29], three different values of rotation of the cochlea (84 rpm, 42 rpm, and 21 rpm) and three different values of the rotation speed of the tool (1600 rpm, 1250 rpm, and 915 rpm) were selected (Table 3). Three tests were performed for each combination of process parameters.

All the tests were carried out with a distance between the cochlea head and the tool equal to 30 mm. The hydraulic system, which causes longitudinal movement of the cochlea, applied a constant load of 5 kN during the productive phase. To overcome typical issues during the run-up phase, a systematic procedure was established (Fig. 4). In particular, after the introduction of a pre-determined amount of chips (i.e. 55 g), the cochlea was put in rotation with a speed equal to 10 % of the assigned speed. At the same time, the tool was put in rotation with the assigned speed, and a load equal to 50 kN, constant for all the case studies, was given to the cochlea.

It is worth noting that the start-up load of 50 kN is fundamental to increasing the relative density of the material confined in the extrusion chamber, as some of the authors have shown that the extrusion process starts only when the relative density of the material close to the tool surface is equal to 1 [11]. After the material reaches the correct conditions of temperature, pressure, and deformation, the start of extrusion is observed.

A first evaluation of the quality of the product was made by visual inspection of the outer surface of the extrudates. The longitudinal view of wires far from the transient start-up zone was analyzed. Specimens were taken from each wire to evaluate the mechanical properties through quasi-static tensile tests, following ASTM D2256, using a

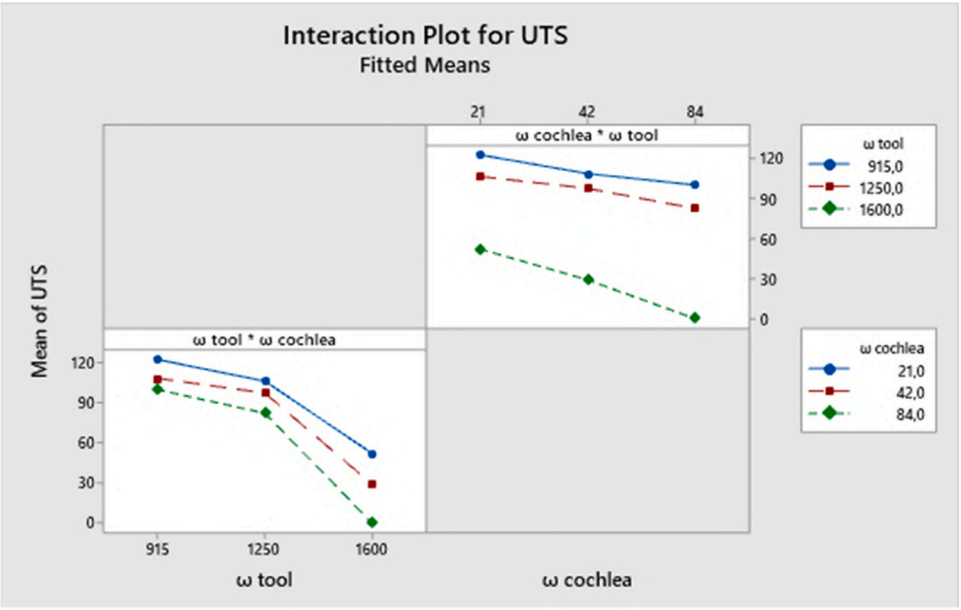

Fig. 14. ANOVA results: interaction between ω tool and ω cochlea for UTS.

Table 5
ANOVA analysis results for ETF% value.

Source	DF	Adj SS	Adj MS	F-Value	P-Value
ω tool	2	464,187	232,093	17612,48	0,000000
ω cochlea	2	36,727	18,363	1393,51	0,000000
ω tool* ω cochlea	4	26,633	6658	505,27	0,000000
Error	18	0237	0013		
Total	26	527,784			

Galdabini Sun 5. Further samples underwent characterization using an Olympus GX 51 optical microscope (OM) and a Phenom ProX Desktop was utilized for scanning electron microscopy (SEM) analyses. Micromechanical characterization in terms of microhardness was determined using a Remet HBV 30. Standard metallographic techniques, such as polishing (alumina diluted in distilled water) and grounding, were employed to prepare the samples. The specimens were then etched for 30 s using Weck's reagent (1 g NaOH, 4 g $KMnO_4$, and 100 ml H_2O) to expose the microstructure. To conduct microhardness testing, a 500 g weight was used to make an indentation in the center of the wires. Additionally, four indentations were made at 0.6 mm intervals from the center, equally spaced on the circumference.

2.2. FEM model

The numerical model of the CFSE process, validated by authors in a previous paper [35], was established using the commercial software SFTC DEFORM 3D™. Tool, cochlea, and chamber were modeled as rigid parts with a mesh of 25,000, 20,000, and 20,000 elements, respectively. For simplicity, the chips were modeled as a porous billet, characterized through the Shime and Oyane plastic model, having an initial relative density of 0.44 and a mesh of 15,000 elements; a refined mesh window

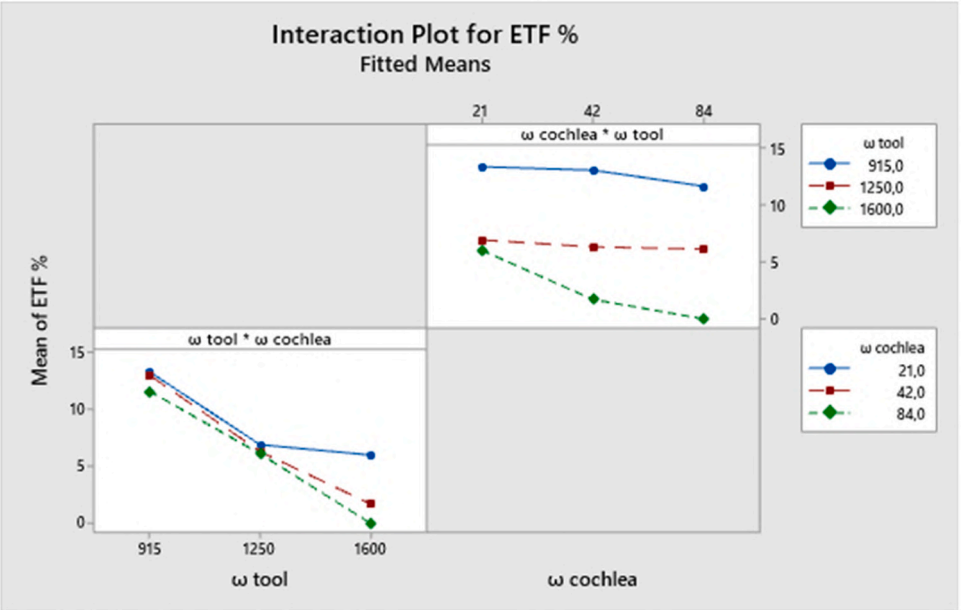

Fig. 15. ANOVA results: interaction between ω tool and ω cochlea for ETF%.

Table 6
ANOVA analysis results for central (a) and radial (b) HV value.

	Source	DF	Adj SS	Adj MS	F-Value	P-Value
a)	ω tool	2	2528,00	1264,00	124873,77	0,000000
	ω cochlea	2	4166,00	2083,00	205784,85	0,000000
	ω tool* ω cochlea	4	3050,00	762,50	75329,31	0,000000
	Error	18	0,18	0,01		
	Total	26	9744,18			
b)	**Source**	**DF**	**Adj SS**	**Adj MS**		
	ω tool	2	2061,25	1030,62	27812,92	0,000000
	ω cochlea	2	4158,17	2079,08	56107,20	0,000000
	ω tool* ω cochlea	4	3603,39	900,85	24310,75	0,000000
	Error	18	0,67	0,04		
	Total	26	9823,47			

was generated in the tool-billet surface contact and along the extrusion hole. A constant shear factor equal to 0.4 was used to model the friction between the rigid parts and the porous billet [36]. The interface heat transfer coefficient was considered equal to 11 N/sec/mm/C for the billet while as the exchange with the environment is concerned, the temperature and the convection coefficient were imposed equal to 20 °C and 0.02 N/sec/mm/C, respectively. The process parameters used in the numerical simulations were defined referring to the experimental tests. Fig. 5 shows the developed model with the meshed "workpiece" at the beginning of the simulation.

3. Results and discussion

3.1. Experimental Results

Fig. 6 shows the process window obtained from the proposed experimental campaign.

As it can be seen, all the combinations of process parameters selected allowed the production of a wire, case study i being the only exception. For this condition, the cochlea required an excessive amount of torque, overcoming the machine's limiting value. The causes for this behavior will be discussed in the next paragraphs. For all the sound case studies, the extrusion process was stopped after that an average wire length of 700 mm was extruded.

Early assessment of product quality is possible by observing the outer surface of the wires (Fig. 7).

It is possible to notice distortions when the tool rotation increases at a set cochlea rotation, e.g. when cochlea rotation is equal to 21 rpm

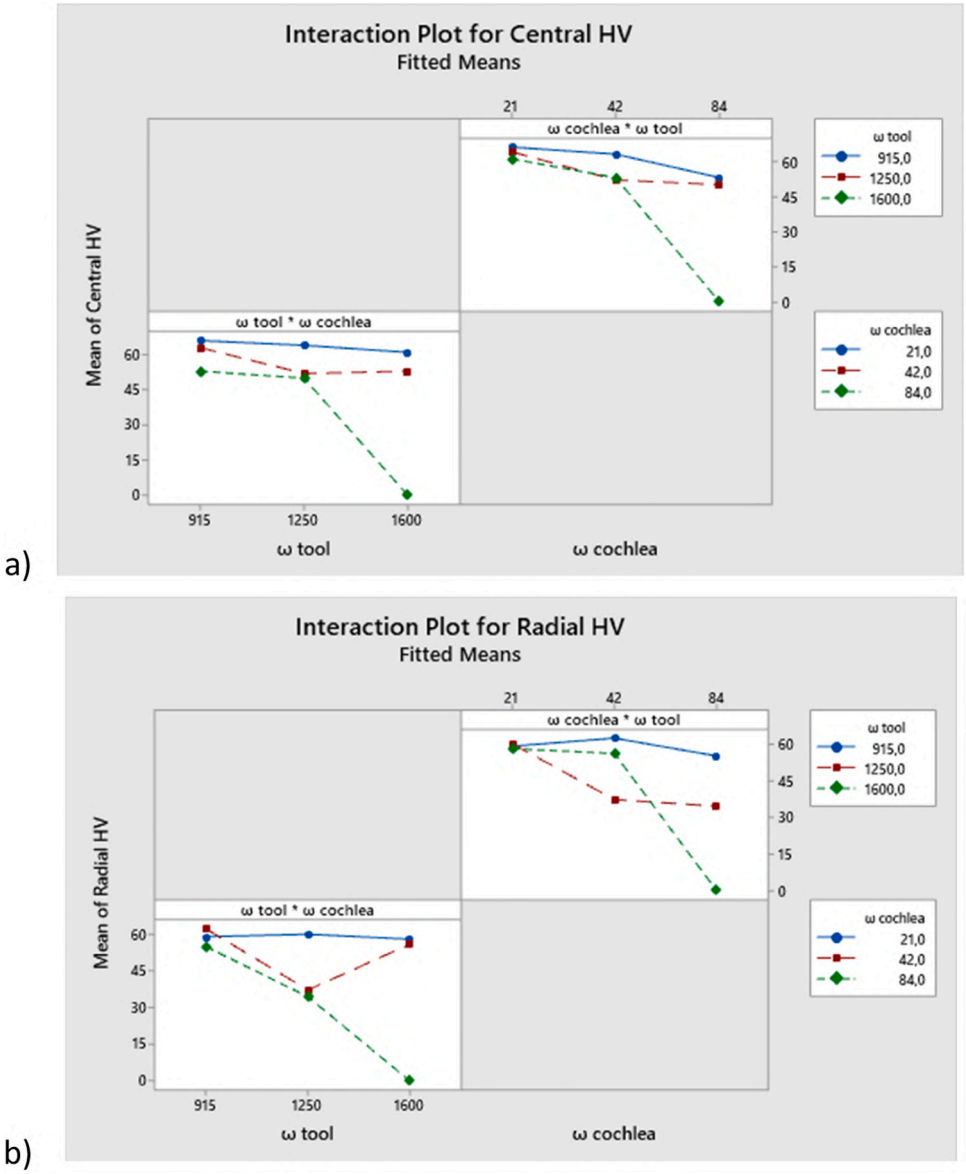

Fig. 16. ANOVA results: interaction between ω tool and ω cochlea for (a) central and (b) radial HV.

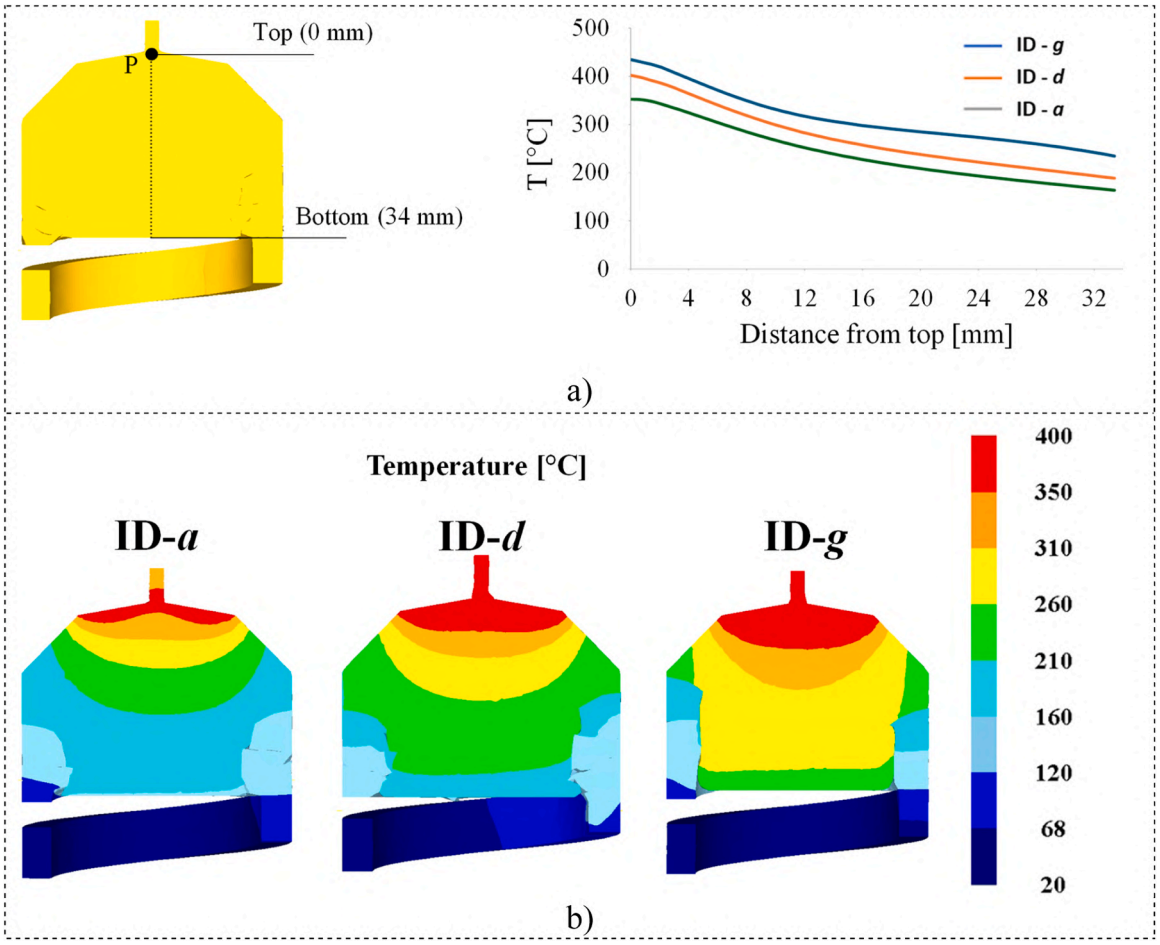

Fig. 17. (a) temperature profile in the billet as a function of the distance from the bottom surface of the tool and (b) temperature distribution in a longitudinal section for case studies ID-a, ID-d, and ID-g.

(Fig. 7a-d-g), or 42 rpm (Fig. 7b-e-h). In turn, with fixed tool rotation of 915 rpm and 1250 rpm, and increasing cochlea rotation, it is possible to observe a more consistent external surface. Finally, as the tool rotation increases up to 1600 rpm, an extremely irregular surface as well as the beginning of hot cracking can be observed (Fig. 7g-h).

First, the mechanical properties of the wires were investigated. Fig. 8 illustrates the Ultimate Tensile Strength (UTS) of the manufactured wires, correlating with both the rotational speed of the cochlea and the rotational speed of the rotating die.

As far as the sound extrudates are concerned, it is possible to observe decreasing UTS values as the rotational speed of the cochlea increases with fixed tool rotation. This trend holds true for the three considered tool rotation values. It is also observed that the reduction in UTS is more significant when the tool rotation increases from 1250 rpm to 1600 rpm. Moreover, a decreasing trend is also observed for increasing cochlea rotation with fixed tool rotation. The maximum value of UTS, equal to 122 MPa, corresponds to 77 % of UTS of the as-cast material (A356-F). As a matter of fact, similarly to FSW, the CFSE process induces a local thermal treatment of the material resulting in the loss of the initial T6 condition [37]. The maximum value is found for the combination of the slowest process parameters of the proposed campaign, i.e. tool rotation of 1200 rpm and cochlea rotation of 21 rpm. As the tool rotation increases, the UTS drastically drops reaching the minimum values with tool rotation equal to 1600 rpm.

The elongation to fracture was also examined in relation to the rotational speed of the cochlea and the tool (Fig. 9).

It is seen a similar trend to the one observed for UTS, as a rapid decrease in the ETF occurs with increasing tool rotation and fixed cochlea rotation for all the three values considered in this study. As the best-performing case studies are considered, it is noted that ETF is higher than the one of the parent materials.

To understand the results and trends obtained during the tensile tests, further characterization was carried out. Fig. 10 shows, for each wire produced, the Vickers hardness value measured at the center of the cross-section and the average value of the hardness measured over a circumference of a radius of 0.6 mm (indentations are indicated in the figure).

Consistently with what was found for UTS, decreasing hardness values are observed as the tool rotation increases with fixed cochlea rotation. It is also noted that radial hardness is characterized by a higher variability than the center hardness. This is due to the peculiar material flow that occurs during the process. Some of the authors have already demonstrated that a helicoidal material flow takes place caused by concurrent effects of the tool rotation and the extrusion speed. [27,35]. In this way, the material advancing front moves on a plane with a certain angle, depending on the considered process parameters, with respect to the cross-section plane [27,35]. It is also noted that relatively high hardness is found for the ID-d, ID-g, and ID-h case studies, which, in turn, are characterized by low UTS and ETF. SEM analyses of the fracture surfaces have been carried out for specimens obtained with increasing tool rotation and fixed cochlea rotation. Fig. 11 shows the fracture surfaces of ID-a, ID-d, and ID-g tests.

The ID-a case experienced a ductile fracture, as shown by the presence of dimples, while the ID-d case showed ductile and brittle fracture zones and the ID-g case showed an entirely brittle fracture surface. Additionally, the presence of internal defects in the longitudinal section

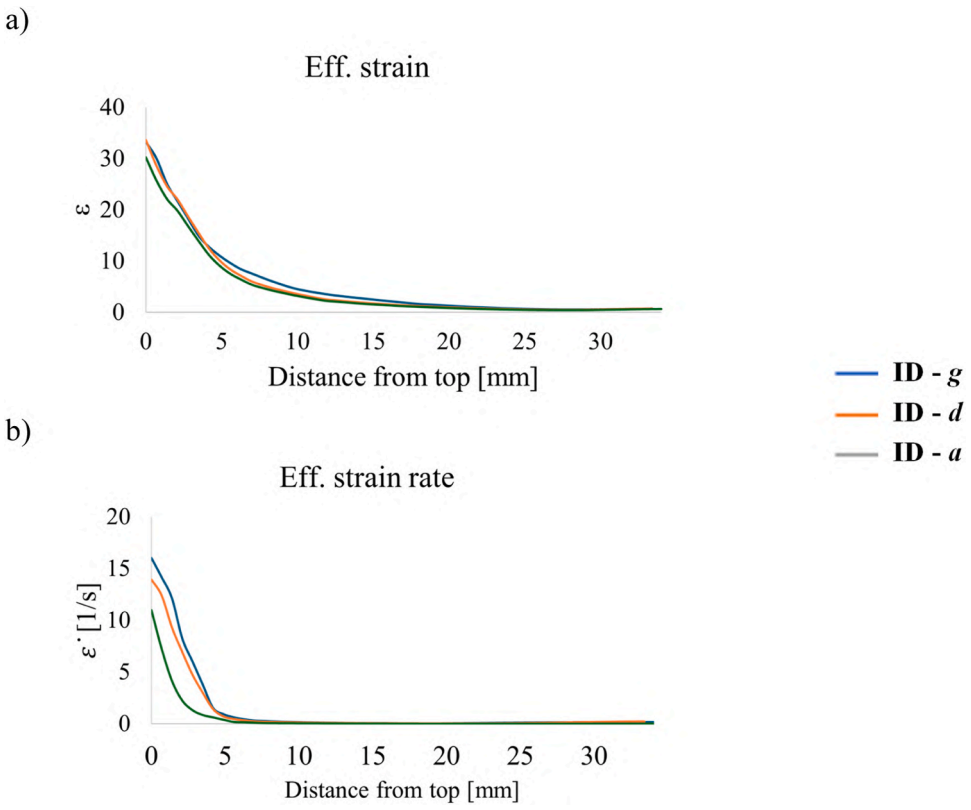

Fig. 18. Comparison of (a) Effective Strain and (b) Effective Strain Rate for Cases ID-a, ID-d, and ID-g.

(Fig. 12), consisting of large void areas (yellow line in Fig. 12), makes clear why, with increasing tool rotation, high hardness, and low UTS and ETF are obtained. During the tensile test, the internal cracks propagate rapidly, resulting in the brittle failure of the cases considered. The causes for the UTS decrease when tool rotation and cochlea rotation increase will be discussed in the FEM results section.

Finally, For the same case studies, SEM analysis was conducted to determine the average grain size (Fig. 13a), through the intercept method, in both the central area and the external one (Fig. 13b). It is noted (Fig. 13c) that increasing grain size is obtained with increasing tool rotation, due to the higher heat input. The external area is characterized by a slightly lower average grain size due to the thermal exchange with the tool. It is worth noting that a similar trend, i.e. increasing average grain size with increasing tool rotation and fixed cochlea rotation, was found for the other cochlea rotation values.

The obtained results highlighted that the Ultimate Tensile Strength (UTS) decreases with increasing tool rotation and cochlea rotation. Notably, the highest value of UTS achieved was approximately 77 % of that of the parent material in its F state. Additionally, the maximum Elongation to Failure (ETF) recorded was 11 %, surpassing that of the parent material. This enhancement in ETF can primarily be attributed to the formation of recrystallized grains that emerged after the processing phase, contrasting markedly with the structure of the as-fabricated parent material. Moreover, the hardness (HV) trends mirrored those of the UTS. Specifically, at elevated tool rotation speeds, the material exhibits a more brittle behavior. This brittleness is due to the presence of significant void defects, which, in spite of the corresponding higher HV values, leads to poor mechanical resistance. Such observations emphasize the complex interplay between mechanical properties and the parameters controlling the manufacturing process, revealing crucial insights into material behavior under varied processing conditions. What has been found is consistent as it is comparable with the results observed by Gumaste et al. [22] in the study of continuous extrusion of feedstock. In order to better highlight the effect of the considered process parameters and their interaction on the main mechanical properties, ANOVA analyses were carried out for UTS, ETF, and microhardness. Table 4 shows the ANOVA analysis results. It is observed that tool rotation (ω tool) and cochlea rotation (ω cochlea) have a significant impact on UTS, with a p-value much lower than the common significance level of 0.05. Hence, variations in these parameters determine a significant difference in UTS levels. Also, the interaction between ω tool and ω cochlea is significant, as demonstrated by the p-value, indicating that the effect of one factor depends on the level of the other factor.

Fig. 14 shows the interaction between ω tool and ω cochlea for UTS. Non-parallel lines indicate an interaction between the two factors, i.e. the effect of increasing ω cochlea depends on the level of ω tool. At low levels of ω tool, UTS is higher with low levels of ω cochlea, whereas at high levels of ω tool, UTS is significantly lower for all levels of ω cochlea.

Table 5 shows ANOVA analysis results performed on the ETF obtained from the mechanical analysis. The same p-values are obtained for the three factors. This suggests that there are significant differences in ETF % for different levels of ω tool and ω cochlea. The interaction between ω tool and ω cochlea is significant, again indicating that the effect of one factor depends on the level of the other factor.

The non-parallel lines in the interaction plot suggest a significant interaction between the two factors (Fig. 15). For instance, the effect of increasing ω cochlea varies depending on the level of ω tool. At lower levels of ω tool, ETF % is higher for lower levels of ω cochlea, whereas at higher levels of ω tool, ETF % significantly decreases for all levels of ω cochlea. The analyses carried out allowed to assess the high influence of tool and cochlea rotation on the mechanical integrity of the final wire. In this way, the correct choice of these process parameters, as well as the full comprehension of their role in the process mechanics, as it will be shown in the next paragraph, is crucial to an effective process design.

Finally, Table 6 shows ANOVA analysis results performed on the central and radial HV values measured. As expected, ω tool and ω cochlea significantly affect HV with a p-value far below the conventional

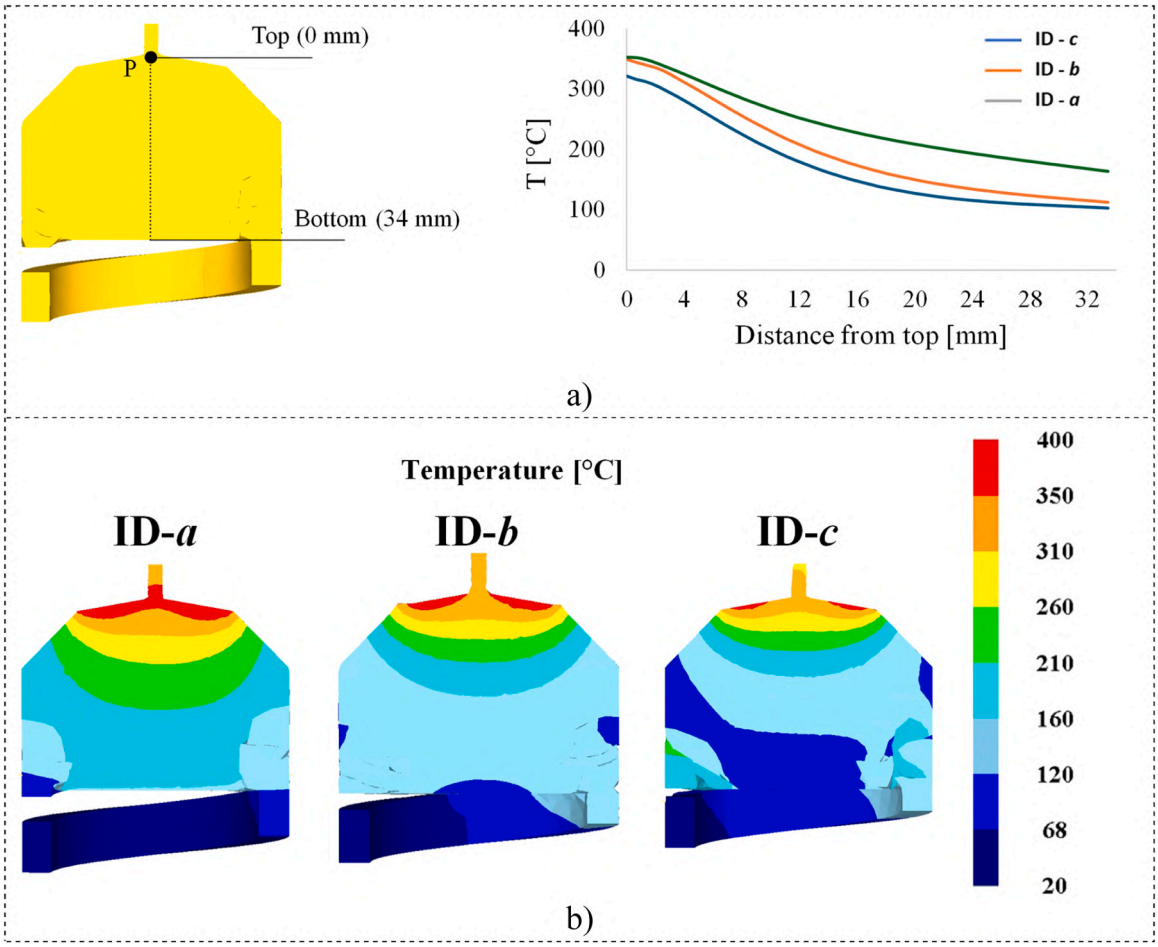

Fig. 19. (a) temperature profile in the billet as a function of the distance from the bottom surface of the tool and (b) temperature distribution in a longitudinal section for case studies ID-a, ID-b, and ID-c.

significance level of 0.05. The interaction between ω tool and ω cochlea is also significant.

Fig. 16a and b show the interaction between process variables for central and radial HV, respectively. At lower levels of ω tool, central HV is higher for lower levels of ω cochlea, whereas at higher levels of ω tool, central HV significantly decreases for all levels of ω cochlea.

3.2. Numerical results

The numerical model was used for a more in-depth understanding of the mechanical properties trends experimentally obtained, allowing the analysis of the effect of the process parameters on the main field variables, i.e. temperature, strain, and strain rate. In particular, it is known that the effectiveness of solid bonding phenomena can be quantitatively evaluated through the Piwnik-Plata criterion (Eq. 2) [38], which depends on the temperature and pressure history the material undergoes.

$$W_c = \int \frac{p}{\sigma_f} dt \tag{2}$$

Where p is the contact pressure at the interface between two adjoining chips and can be considered as the mean stress in the modeled porous material; σ_f is the flow stress of the material in the given temperature, strain, and strain rate conditions.

Temperatures were calculated along the billet axis during the extrusion process. Fig. 17 shows the temperature profile in the billet as a function of the distance from the bottom surface of the tool as well as the temperature distribution in a longitudinal section, for the case studies ID-a, ID-d, and ID-g, i.e. for fixed cochlea rotation equal to 21 rpm and varying tool rotation. As expected, the temperature of the material close to the bottom surface of the tool increases as the cochlea rotation increases, resulting in a significantly larger Heat Affected Zone (HAZ).

In Fig. 18 a and b it is possible to observe the strain and strain rate profiles, respectively, calculated at the same points considered for temperature in Fig. 17a. First, it is noted that, regardless of the considered tool rotation, the material is affected by the tool rotation in an area characterized by a height of about 16 mm. For longer distances from the tool bottom surface, no significant effective strain is calculated.

Then, a slight increase in both strain and strain rate is observed with increasing tool rotation. The local values of temperature, strain, and strain rate have been used to calculate the material flow stress for each point. The values of W obtained for point P (see again Fig. 17a), laying along the wire axis at the tool bottom surface when the extrusion process begins, are 3.55 for ID-a, 3.36 for ID-d, and 3.12 for the ID-g case. It is worth noticing that, in order to calculate these values, the considered point was tracked during the process recording the history of all the field variables values, according to the procedure followed in [39,40]. It is worth noting that the Piwnik-Plata criterion was not implemented across the entire analysis field. Instead, field variables were obtained for 10 track points, and these variables were then used to evaluate the weld quality. This approach, focusing on selected track points to derive critical welding parameters, aligns with methodologies previously utilized in the analysis of Friction Stir Welding, as detailed in reference [11]. The experimental and numerical results make clear the decreasing trend obtained for UTS and ETF with fixed cochlea rotation and increasing tool rotation. Indeed, with increasing tool rotation, temperature increases, leading to grain growth. Additionally, with increasing tool rotation, the

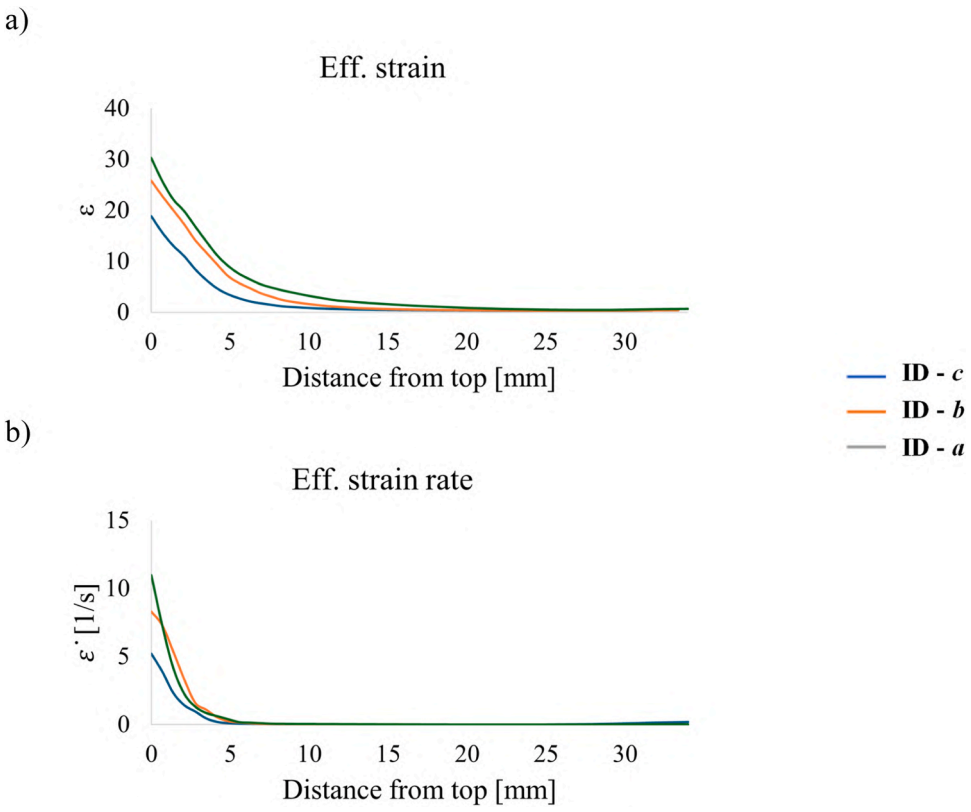

Fig. 20. Comparison of (a) Effective Strain and (b)Effective Strain Rate for Cases ID-a, ID-b, and ID-c.

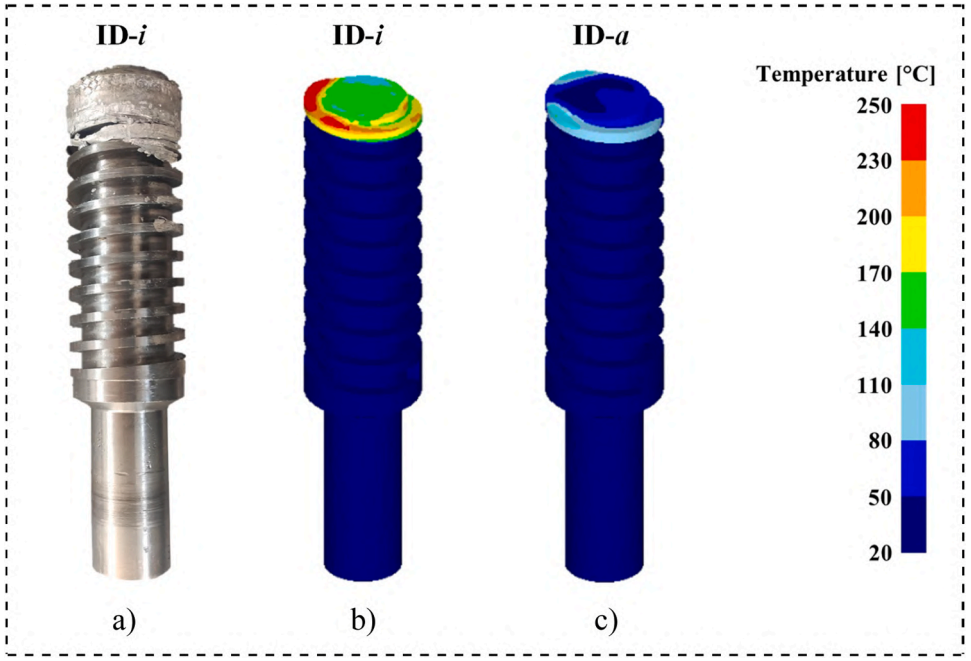

Fig. 21. (a) consolidated material on the cochlea at the end of the process for failed case study. Temperature distribution calculated in the cochlea during (b) failed case study and (c) proper cochlea operation.

combined effect of (i) the increasing temperature, resulting in decreasing material flow stress, and (ii) decreasing stress, results in lower values of W, i.e. lower solid bonding quality.

A similar approach was followed to investigate the effect of the cochlea rotation on the mechanical properties. In Fig. 19, temperature profiles and distributions are shown for case studies ID-a, ID-b, and ID-c. It can be seen that temperature gradually increases with decreasing cochlea rotation. In particular, higher cochlea rotation leads to a higher extrusion rate. In this way, due to quicker heat dissipation, the material in the region of the extrusion chamber is colder, and thinner thermal layers are observed (Fig. 19b).

In Fig. 20 a and b the strain and strain rate profiles, calculated as

described for Fig. 18, are shown. An increase in the cochlea rotation results in lower values of strain and strain rate all along the billet axis (Fig. 18a and b). This is due to the higher extrusion rate caused by the faster material supply by the cochlea. In this way, a single material particle rotates less around the billet longitudinal axis and accumulates less strain. The combined effect of lower temperature, and lower time results in lower values of the Piwnik-Plata W. The obtained values of W for point P (Fig. 19a) are 3.55 for ID-a, 3.01 for ID-b, and 2.52 for the ID-c case, indicating decreasing bonding quality with increasing cochlea rotation. The reduced material mixing and the lower values of W obtained with higher cochlea rotation can explain the significant drop in the UTS experimentally observed for any given tool rotation.

The numerical model was used also to understand the reasons for the failed test ID-i, for which the maximum tool and cochlea rotation values, among the ones considered in this study, are selected. As the temperature distribution in the cochlea is observed (Fig. 21 b and c), it is seen that the cochlea top area, i.e. the one close to the extrusion chamber, has a higher temperature. This is due to the concurrent effect of the high tool rotation and high cochlea rotation, whose top surface acts as a "secondary tool" creating heat by friction. In these conditions, the chips do not consolidate just close to the tool surface, but consolidation rather starts close to the cochlea end (Fig. 21a). This creates a "block" to incoming chips that cannot reach the tool, thus leading to process failure. When such a condition takes place the torque on the cochlea measured by the FSE machine increases reaching the machine limit.

4. Summary and conclusions

In this study, A356-T6 aluminum alloy chips were directly recycled through the CFSE solid-state process. An experimental campaign was carried out to investigate the effect of the main CFSE process parameters on the produced wires' mechanical properties. The experimental campaign plan included 9 case studies, each involving three levels of tool rotation and three levels of cochlea rotation. For each case study, tensile tests, Vickers hardness, fracture surface analysis, internal material flow, and average grain size were investigated. A dedicated numerical model, previously validated, was used to predict the distribution of the main field variables, namely temperature, strain, and strain rate, to understand the results observed during tensile and microhardness tests. The Piwnik-Plata criterion was used to numerically predict the soundness of the solid bonding achieved for each case study.

Based on the obtained results, the following main conclusion can be drawn:

- ✓ Decreasing UTS was obtained with increasing tool rotation and cochlea rotation; the maximum UTS obtained was equal to 77 % of the parent material in the F state; the maximum ETF obtained was equal to 11 %, which is larger than the one of the parent material. This is due to the recrystallized grain obtained after the process as compared to the as-cast parent material structure.
- ✓ Anova analyses highlighted the strong influence of each considered process parameter as well as their interaction on UTS, ETF and microhardness.
- ✓ The HV trend generally follows the UTS one. For large values of tool rotation, a brittle behavior, characterized by large void defects and larger HV values, is observed.
- ✓ With fixed cochlea rotation, increasing tool rotation leads to both larger average grain size and lower calculated Piwnik-Plata parameter W, indicating lower quality of the solid bonding process explaining the UTS trend observed experimentally.
- ✓ With fixed tool rotation, increasing cochlea rotation leads to both low values of strain, i.e. material stirring, and higher extrusion rates. In turn, the latter results in lower process times and hence lower Piwnik-Plata parameter W.
- ✓ For the failed case study ID-i, it was found that the combined effect of high tool and cochlea rotation caused the chips' temperature to increase close to the cochlea. Consequently, material consolidation occurred in that area creating an obstacle for the incoming chips and thus leading to cochlea torque increase and process failure.

Although the above analysis and conclusions are for the A356 aluminum alloy, the present experimental and numerical approach can be used with different chip materials, thus providing an effective tool for proper CFSE process design. Future work will be focused on the wire mechanical properties optimization through the use of AI tools on a wider range of variations of the considered process parameters.

Funding

This study was carried out within the MICS (Made in Italy – Circular and Sustainable) Extended Partnership and received funding from the European Union Next-Generation EU (PIANO NAZIONALE DI RIPRESA E RESILIENZA (PNRR) – MISSIONE 4 COMPONENTE 2, INVESTIMENTO 1.3 – D.D. 1551.11–10–2022, PE00000004). This manuscript reflects only the authors' views and opinions, neither the European Union nor the European Commission can be considered responsible for them.

CRediT authorship contribution statement

Riccardo Puleo: Software, Formal analysis. **Livan Fratini:** Supervision, Project administration, Methodology, Funding acquisition, Conceptualization. **gianluca buffa:** Writing – review & editing, Writing – original draft, Supervision, Project administration, Methodology, Conceptualization. **Simone Amantia:** Writing – original draft, Visualization, Validation, Investigation. **Davide Campanella:** Writing – original draft, Visualization, Supervision, Methodology, Conceptualization.

Declaration of Competing Interest

The authors declare that they have no known competing financial interests or personal relationships that could have appeared to influence the work reported in this paper.

References

[1] Worrell E, Allwood J, Gutowski T. The role of material efficiency in environmental stewardship. Annu Rev Environ Resour 2016;41:575–98. https://doi.org/10.1146/annurev-environ-110615-085737.

[2] Gutowski TG, Sahni S, Allwood JM, Ashby MF, Worrell E. The energy required to produce materials: constraints on energy-intensity improvements, parameters of demand. Philos Trans R Soc A: Math, Phys Eng Sci 2013;371. https://doi.org/10.1098/rsta.2012.0003.

[3] Tolio T, Bernard A, Colledani M, Kara S, Seliger G, Duflou J, et al. Design, management and control of demanufacturing and remanufacturing systems. CIRP Ann Manuf Technol 2017;66:585–609. https://doi.org/10.1016/j.cirp.2017.05.001.

[4] Atherton J. Declaration by the metals industry on recycling principles. Int J Life Cycle Assess 2007;12:59–60. https://doi.org/10.1065/lca2006.11.283.

[5] Ingarao G. Manufacturing strategies for efficiency in energy and resources use: the role of metal shaping processes. J Clean Prod 2017;142:2872–86. https://doi.org/10.1016/j.jclepro.2016.10.182.

[6] Wan B, Chen W, Lu T, Liu F, Jiang Z, Mao M. Review of solid state recycling of aluminum chips. Resour Conserv Recycl 2017;125:37–47. https://doi.org/10.1016/j.resconrec.2017.06.004.

[7] Cooper DR, Allwood JM. The influence of deformation conditions in solid-state aluminium welding processes on the resulting weld strength. J Mater Process Technol 2014;214:2576–92. https://doi.org/10.1016/j.jmatprotec.2014.04.018.

[8] Paraskevas D, Vanmeensel K, Vleugels J, Dewulf W, Deng Y, Duflou JR. Spark plasma sintering as a solid-state recycling technique: The case of aluminum alloy scrap consolidation. Materials 2014;7:5664–87. https://doi.org/10.3390/ma7085664.

[9] Tekkaya AE, Schikorra M, Becker D, Biermann D, Hammer N, Pantke K. Hot profile extrusion of AA-6060 aluminum chips. J Mater Process Technol 2009;209:3343–50. https://doi.org/10.1016/j.jmatprotec.2008.07.047.

[10] Liu G, Bangs CE, Müller DB. Stock dynamics and emission pathways of the global aluminium cycle. Nat Clim Chang 2013;3:338–42. https://doi.org/10.1038/nclimate1698.

[11] Baffari D, Buffa G, Fratini L. A numerical model for wire integrity prediction in friction stir extrusion of magnesium alloys. J Mater Process Technol 2017;247:1–10. https://doi.org/10.1016/j.jmatprotec.2017.04.007.
[12] Baffari D, Buffa G, Campanella D, Fratini L, Reynolds AP. Process mechanics in friction stir extrusion of magnesium alloys chips through experiments and numerical simulation. J Manuf Process 2017;29:41–9. https://doi.org/10.1016/j.jmapro.2017.07.010.
[13] Baffari D, Reynolds AP, Masnata A, Fratini L, Ingarao G. Friction stir extrusion to recycle aluminum alloys scraps: energy efficiency characterization. J Manuf Process 2019;43:63–9. https://doi.org/10.1016/J.JMAPRO.2019.03.049.
[14] Jamali G, Nourouzi S, Jamaati R. Microstructure and mechanical properties of AA6063 aluminum alloy wire fabricated by friction stir back extrusion (FSBE) process. Int J Miner, Metall Mater 2019;26:1005–12. https://doi.org/10.1007/s12613-019-1806-9.
[15] Jamali G, Nourouzi S, Jamaati R. FSBE process: a technique for fabrication of aluminum wire with randomly oriented fine grains. Mater Lett 2019;241:68–71. https://doi.org/10.1016/j.matlet.2019.01.049.
[16] Tahmasbi K, Mahmoodi M, Tavakoli H. Corrosion resistance of aluminum alloy AA7022 wire fabricated by friction stir extrusion. Trans Nonferrous Met Soc China (Engl Ed) 2019;29:1601–9. https://doi.org/10.1016/S1003-6326(19)65067-3.
[17] Tahmasbi K, Mahmoodi M. Evaluation of microstructure and mechanical properties of aluminum AA7022 produced by friction stir extrusion. J Manuf Process 2018;32:151–9. https://doi.org/10.1016/J.JMAPRO.2018.02.008.
[18] Abdi Behnagh R, Samanta A, Agha Mohammad Pour M, Esmailzadeh P, Ding H. Predicting microstructure evolution for friction stir extrusion using a cellular automaton method. Model Simul Mat Sci Eng 2019;27. https://doi.org/10.1088/1361-651X/ab044b.
[19] Akbari M, Asadi P. Optimization of microstructural and mechanical properties of brass wire produced by friction stir extrusion using Taguchi method. Proc Inst Mech Eng, Part L: J Mater: Des Appl 2021;235:2709–19. https://doi.org/10.1177/14644207211032992.
[20] Asadi P., Akbari M. Numerical modeling and experimental investigation of brass wire forming by friction stir back extrusion n.d. ⟨https://doi.org/10.1007/s00170–021-07729–5/Published⟩.
[21] Asadi P, Akbari M, Talebi M, Peyghami M, Sadowski T, Aliha MRM. Production of LM28 tubes by mechanical alloying and using friction stir extrusion. Page 814 2023;13 Crystals 2023;Vol 13:814. https://doi.org/10.3390/CRYST13050814.
[22] Gumaste A, Haridas RS, Gupta S, Gaddam S, Kandasamy K, McWilliams BA, et al. Solid stir extrusion: innovating friction stir technology for continuous extrusion process. J Mater Process Technol 2023;316:117952. https://doi.org/10.1016/J.JMATPROTEC.2023.117952.
[23] Li J, Meng X, Li Y, Wan L, Huang Y. Friction stir extrusion for fabricating Mg-RE alloys with high strength and ductility. Mater Lett 2021;289. https://doi.org/10.1016/j.matlet.2021.129414.
[24] Li L, Gupta V, Li X, Reynolds AP, Grant G, Soulami A. Meshfree simulation and experimental validation of extreme thermomechanical conditions in friction stir extrusion. Comput Part Mech 2022;9:789–809. https://doi.org/10.1007/s40571-021-00445-7.
[25] Jarrah OM, Nazzal MA, Darras BM. Numerical modeling and experiments of friction stir back extrusion of seamless tubes. CIRP J Manuf Sci Technol 2020;31:165–77. https://doi.org/10.1016/J.CIRPJ.2020.11.001.
[26] Jamali G, Nourouzi S, Jamaati R. Manufacturing of gradient Al/SiC composite wire by friction stir back extrusion. CIRP J Manuf Sci Technol 2021;35:735–43. https://doi.org/10.1016/j.cirpj.2021.09.004.
[27] Widerøe F, Welo T. Using contrast material techniques to determine metal flow in screw extrusion of aluminium. J Mater Process Technol 2013;213:1007–18. https://doi.org/10.1016/j.jmatprotec.2012.11.013.
[28] Skorpen KG, Roven HJ, Reiso O. A physical based empirical model for the accumulated strain in novel metal continuous screw extrusion (MCSE). J Mater Process Technol 2020;282. https://doi.org/10.1016/j.jmatprotec.2020.116670.
[29] Buffa G, Campanella D, Micari F, Fratini L. Design and development of a new machine tool for continuous friction stir extrusion. CIRP J Manuf Sci Technol 2023;41:391–400. https://doi.org/10.1016/j.cirpj.2023.01.004.
[30] Brandl E, Baufeld B, Leyens C, Gault R. Additive manufactured Ti-6Al-4V using welding wire: comparison of laser and arc beam deposition and evaluation with respect to aerospace material specifications. Phys Procedia 2010;5:595–606. https://doi.org/10.1016/J.PHPRO.2010.08.087.
[31] Joseph R. Davis. Aluminum and Aluminum Alloys. 1993.
[32] Davis J.R., Allen P., Lampman S.R., Zorc T.B., Henry S.D., Daquila J.L., et al. ASM HandbooK, Volume 2, Properties and Selection: Nonferrous Alloys and Special-Purpose materials. 2012.
[33] La Torre EADe, Pérez-Bustamante R, Camarillo-Cisneros J, Gómez-Esparza CD, Medrano-Prieto HM, Martínez-Sánchez R. Mechanical properties of the A356 aluminum alloy modified with La/Ce. J Rare Earths 2013;31:811–6. https://doi.org/10.1016/S1002-0721(12)60363-9.
[34] Kimura T, Nakamoto T. Microstructures and mechanical properties of A356 (AlSi7Mg0.3) aluminum alloy fabricated by selective laser melting. Mater Des 2016;89:1294–301. https://doi.org/10.1016/J.MATDES.2015.10.065.
[35] Buffa G, Campanella D, Micari F, Fratini L. Design and development of a new machine tool for continuous friction stir extrusion. CIRP J Manuf Sci Technol 2023;41:391–400. https://doi.org/10.1016/j.cirpj.2023.01.004.
[36] Buffa G, Hua J, Shivpuri R, Fratini L. A continuum based fem model for friction stir welding - model development. Mater Sci Eng A 2006;419:389–96. https://doi.org/10.1016/j.msea.2005.09.040.
[37] Baffari D, Reynolds AP, Li X, Fratini L. Influence of processing parameters and initial temper on friction stir extrusion of 2050 aluminum alloy. J Manuf Process 2017;28:319–25. https://doi.org/10.1016/j.jmapro.2017.06.013.
[38] Bocchi S, D'Urso G, Giardini C. Numerical modeling of a sustainable solid-state recycling of aluminum scraps by means of friction stir extrusion process. Materials 2023;16:4375. https://doi.org/10.3390/ma16124375.
[39] Puleo R, Latif A, Ingarao G, Di Lorenzo R, Fratini L. Solid bonding criteria design for aluminum chips recycling through friction stir consolidation. J Mater Process Technol 2023;319:118080. https://doi.org/10.1016/j.jmatprotec.2023.118080.
[40] Baffari D, Buffa G, Fratini L. A numerical model for Wire integrity prediction in friction stir extrusion of magnesium alloys. J Mater Process Technol 2017;247:1–10. https://doi.org/10.1016/j.jmatprotec.2017.04.007.